

# Biodistribution and Radiation Dosimetry of the Integrin Marker $^{18}\text{F}$ -RGD-K5 Determined from Whole-Body PET/CT in Monkeys and Humans

Mohan Doss<sup>1</sup>, Hartmuth C. Kolb<sup>2</sup>, James J. Zhang<sup>2</sup>, Marie-José Bélanger<sup>3</sup>, James B. Stubbs<sup>4</sup>, Michael G. Stabin<sup>5</sup>, Eric D. Hostetler<sup>3</sup>, R. Katherine Alpaugh<sup>6</sup>, Margaret von Mehren<sup>7</sup>, Joseph C. Walsh<sup>2</sup>, Michael Haka<sup>2</sup>, Vani P. Mocharla<sup>2</sup>, and Jian Q. Yu<sup>1</sup>

<sup>1</sup>Diagnostic Imaging, Fox Chase Cancer Center, Philadelphia, Pennsylvania; <sup>2</sup>Biomarker Research, Siemens Molecular Imaging Inc., Culver City, California; <sup>3</sup>Imaging, Merck and Co., West Point, Pennsylvania; <sup>4</sup>Radiation Dosimetry Systems, Inc., Alpharetta, Georgia; <sup>5</sup>Department of Radiology and Radiological Sciences, Vanderbilt University, Nashville, Tennessee; <sup>6</sup>Protocol Support Lab, Fox Chase Cancer Center, Philadelphia, Pennsylvania; and <sup>7</sup>Medical Oncology, Fox Chase Cancer Center, Philadelphia, Pennsylvania

2-((2S,5R,8S,11S)-5-benzyl-8-(4-((2S,3R,4R,5R,6S)-6-((2-(4-(3- $^{18}\text{F}$ -fluoropropyl)-1H-1,2,3-triazol-1-yl)acetamido)methyl)-3,4,5-trihydroxytetrahydro-2H-pyran-2-carboxamido)butyl)-11-(3-guanidinopropyl)-3,6,9,12,15-pentaoxo-1,4,7,10,13-pentaa-zacyclopentadecan-2-yl)acetic acid ( $^{18}\text{F}$ -RGD-K5) has been developed as an  $\alpha_v\beta_3$  integrin marker for PET. The purpose of this study was to determine the biodistribution and estimate the radiation dose from  $^{18}\text{F}$ -RGD-K5 using whole-body PET/CT scans in monkeys and humans. **Methods:** Successive whole-body PET/CT scans were obtained after intravenous injection of  $^{18}\text{F}$ -RGD-K5 in 3 rhesus monkeys ( $167 \pm 19$  MBq) and 4 healthy humans ( $583 \pm 78$  MBq). In humans, blood samples were collected between the PET/CT scans, and stability of  $^{18}\text{F}$ -RGD-K5 was assessed. Urine was also collected between the scans, to determine the total activity excreted in urine. The PET scans were analyzed to determine the radiotracer uptake in different organs. OLINDA/EXM software was used to calculate human radiation doses based on human and monkey biodistributions. **Results:**  $^{18}\text{F}$ -RGD-K5 was metabolically stable in human blood up to 90 min after injection, and it cleared rapidly from the blood pool, with a 12-min half-time. For both monkeys and humans, increased  $^{18}\text{F}$ -RGD-K5 uptake was observed in the kidneys, bladder, liver, and gallbladder, with mean standardized uptake values at 1 h after injection for humans being approximately 20, 50, 4, and 10, respectively. For human biodistribution data, the calculated effective dose was  $31 \pm 1$   $\mu\text{Sv}/\text{MBq}$ , and the urinary bladder wall had the highest absorbed dose at  $376 \pm 19$   $\mu\text{Gy}/\text{MBq}$  using the 4.8-h bladder-voiding model. With the 1-h voiding model, these doses reduced to  $15 \pm 1$   $\mu\text{Sv}/\text{MBq}$  for the effective dose and  $103 \pm 4$   $\mu\text{Gy}/\text{MBq}$  for the absorbed dose in the urinary bladder wall. For a typical injected activity of 555 MBq, the effective dose would be  $17.2 \pm 0.6$  mSv for the 4.8-h model, reducing to  $8.3 \pm 0.4$  mSv for the 1-h model. For monkey biodistribution data, the effective dose to humans would be  $22.2 \pm 2.4$  mSv for the 4.8-h model and  $12.8 \pm 0.2$  mSv for

the 1-h model. **Conclusion:** The biodistribution profile of  $^{18}\text{F}$ -RGD-K5 in monkeys and humans was similar, with increased uptake in the bladder, liver, and kidneys. There was rapid clearance of  $^{18}\text{F}$ -RGD-K5 through the renal system. The urinary bladder wall received the highest radiation dose and was deemed the critical organ. Both whole-body effective dose and bladder dose can be reduced by more frequent voiding.  $^{18}\text{F}$ -RGD-K5 can be used safely for imaging  $\alpha_v\beta_3$  integrin expression in humans.

**Key Words:**  $^{18}\text{F}$ -RGD-K5; biodistribution; internal dosimetry; integrin marker; PET

**J Nucl Med 2012; 53:1–9**

DOI: 10.2967/jnumed.111.088955

**T**umor-induced angiogenesis undoubtedly influences tumor progression. Great efforts are being made to develop antiangiogenic therapeutic strategies that interrupt the angiogenic process to deprive the tumor of necessary nourishment (1). Vital components of the angiogenic process are the  $\alpha_v\beta_3$  integrins, which mediate endothelial cell migration and survival during angiogenesis (2). They are expressed on the endothelial cells, forming potential vasculature structures that aid in supplying nutrients to tumor cells, particularly melanomas. In normal tissues, expression of integrin  $\alpha_v\beta_3$  is highly restricted, making the  $\alpha_v\beta_3$  subtype an attractive target for cancer imaging probes. The imaging of integrin  $\alpha_v\beta_3$  as it relates to angiogenesis could provide early information related to changes in a tumor's response to the antiangiogenesis therapy preceding changes in tumor sizes, which are typically visualized using standard imaging methods such as CT or MRI. With this early biochemical information, nonresponders might avoid the continuation of the ineffective antiangiogenesis therapy, unwanted side effects, and cost associated with the treatment. In addition,  $\alpha_v\beta_3$  expression may be an important prognostic factor in characterizing the invasiveness and malignant potential of tumors, including breast and colon

Received Jul. 25, 2011; revision accepted Jan. 10, 2012.  
For correspondence or reprints contact: Jian Q. Yu, Diagnostic Imaging, Fox Chase Cancer Center, 333 Cottman Ave., Philadelphia, PA 19111.  
E-mail: Michael.Yu@fccc.edu  
Published online ■■■■.  
COPYRIGHT © 2012 by the Society of Nuclear Medicine, Inc.

cancer (3,4). Noninvasive quantification of  $\alpha_v\beta_3$  expression may have the additional potential of characterizing a malignant tumor's aggressiveness, without the need for invasive collection of tissue samples (i.e., tissue biopsy).

Several integrin  $\alpha_v\beta_3$  receptor binding agents have been developed for use in PET. Several of these imaging agents incorporate a cyclic peptide consisting of an Arg-Gly-Asp (RGD) sequence, which is a well-studied integrin-binding pharmacophore.  $^{18}\text{F}$ -galacto-RGD is the most investigated PET tracer for detecting aberrant  $\alpha_v\beta_3$  expression in tumors, showing a favorable biodistribution in humans, with specific receptor binding and visualization of  $\alpha_v\beta_3$  expression in tumors with high contrast (5). However, the radiosynthetic preparation of  $^{18}\text{F}$ -galacto-RGD remains complex, involving multiple synthetic steps that complicate routine production (6). In addition, reducing the liver uptake of these RGD-based imaging agents would help widen the imaging area in patients. 2-((2*S*,5*R*,8*S*,11*S*)-5-benzyl-8-(4-((2*S*,3*R*,4*R*,5*R*,6*S*)-6-((2-(4-(3- $^{18}\text{F}$ -fluoropropyl)-1*H*-1,2,3-triazol-1-yl)acetamido)methyl)-3,4,5-trihydroxytetrahydro-2*H*-pyran-2-carboxamido)butyl)-11-(3-guanidinopropyl)-3,6,9,12,15-penta-oxo-1,4,7,10,13-pentaazacyclopentadecan-2-yl)acetic acid ( $^{18}\text{F}$ -RGD-K5) is also an RGD-based PET integrin radiotracer

[Fig. 1] (Fig. 1) but additionally contains a metabolically stable, yet highly polar, 1,2,3-antitriazole moiety that increases the tracer's excretion via the kidneys into the bladder, thus circumventing unwanted liver uptake. This tracer binds selectively to integrin  $\alpha_v\beta_3$  (dissociation constant = 7.9 nM) over other related integrins. The tracer has preferential tumor uptake in U87MG xenografts, with a tumor-to-muscle ratio of more than 5:1 after 2 h, making  $^{18}\text{F}$ -RGD-K5 a promising tracer for imaging integrin  $\alpha_v\beta_3$  expression in vivo in tumors undergoing aberrant angiogenesis (7). In comparison to  $^{18}\text{F}$ -galacto-RGD, the preparation of  $^{18}\text{F}$ -RGD-K5 is simple and straightforward using click chemistry, consisting of a single reaction that can be readily automated (7).

The main goal of this study was to measure the biodistribution and dosimetry of  $^{18}\text{F}$ -RGD-K5 in humans. A secondary goal was to determine whether biodistribution of  $^{18}\text{F}$ -RGD-K5 in monkeys can adequately predict the biodistribution and dosimetry in humans.

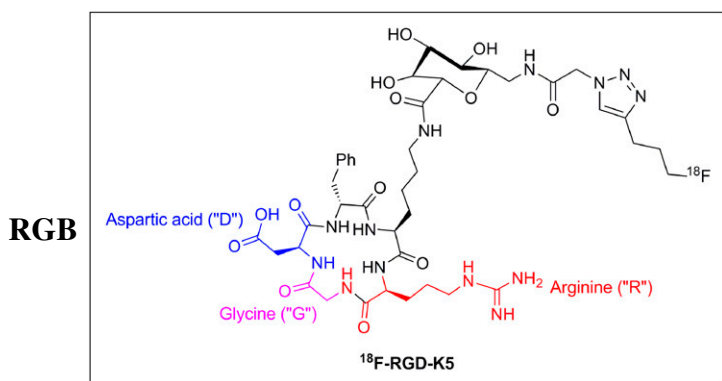


FIGURE 1. Chemical structure of  $^{18}\text{F}$ -RGD-K5.

## MATERIALS AND METHODS

### Radiopharmaceutical Preparation

$^{18}\text{F}$ -RGD-K5 is a triazole-containing RGD peptide useful for detecting  $\alpha_v\beta_3$  integrin expression in vivo.

Production of  $^{18}\text{F}$ -RGD-K5 suitable for human injection was accomplished in 2 steps on an automated synthesis module. First, pentyne tosylate was reacted with  $\text{K}^{18}\text{F}$  in the presence of Kryptofix 222 (Sigma Aldrich),  $\text{K}_2\text{CO}_3$ , and acetonitrile (MeCN) at  $110^\circ\text{C}$  for 10 min. After fluorination, the  $^{18}\text{F}$ -pentyne was distilled into a vial containing RGD-K5- $\text{N}_3$ ,  $\text{CuSO}_4$ , sodium ascorbate, and a copper ligand tris[(1-benzyl-1*H*-1,2,3-triazol-4-yl)methyl]amine in the presence of alcohol (EtOH) and water (Fig. 2). After reacting for 10 min, the crude reaction mixture was purified by reversed-phase high-performance liquid chromatography (HPLC) (MeCN:water with 0.05% trifluoroacetic acid), and the collected fraction was reconstituted as an injectable solution of 10% EtOH:water via C18 trap and release. The final solution was passed through a sterile filter (Pall Corp.). This process produced  $^{18}\text{F}$ -RGD-K5 that was free of Kryptofix 222, pyrogens, and residual solvents (MeCN  $\leq 0.04\%$ ); was sterile; and possessed an acceptable pH profile (pH 5–7.5).

[Fig. 2]

The production of  $^{18}\text{F}$ -RGD-K5 investigational product was conducted according to our Investigational New Drug application (no. 102,075), submitted to the U.S. Food and Drug Administration. Individual doses of  $^{18}\text{F}$ -RGD-K5 contained a maximum of 740 MBq. Each manufactured batch of  $^{18}\text{F}$ -RGD-K5 was formulated to yield a minimum specific activity of more than 14.8 GBq/ $\mu\text{mol}$ . Therefore, a typical individual patient dose contained, by weight, a micro-dose ranging up to a maximum of 50  $\mu\text{g}$  of RGD-K5 per dose.

### Human Subjects

The study was approved by the Research Review Committee, Institutional Review Board, and Radiation Safety Committee of Fox Chase Cancer Center. Four healthy female volunteers (mean age  $\pm$  SD,  $53 \pm 18$  y; age range, 32–75 y) were included in the study. Written informed consent was obtained from each subject. The subjects' weights were  $64 \pm 5$  kg (range, 57–68 kg). All subjects were healthy based on history, physical examination, electrocardiogram, urinalysis, and standard blood tests.

### Human PET/CT Acquisition and Image Analysis

After the intravenous injection of  $^{18}\text{F}$ -RGD-K5 ( $583 \pm 78$  MBq; range, 474–659 MBq) to the volunteers, 5 successive whole-body (WB) PET/CT scans were obtained on a Discovery LS (GE Healthcare) PET/CT scanner. The lowest possible milli-ampere setting on the scanner was used to acquire the CT scans for attenuation correction. The helical CT scan acquisition parameters were 140 kVp, 10 mA, 0.8-s rotation, 5-mm slice thickness, and 4.25-mm interval.

The WB PET scans were acquired in 2-dimensional mode and ranged from the top of the head to mid thigh. The 5 WB scans were acquired at approximately 15, 60, 90, 120, and 140 min after injection. The scan time was 1.5 min per bed position, and each scan covered 7 bed positions, with single-slice overlap between the bed positions. In addition, after the first WB scan, a PET/CT scan of mid thigh to toes was obtained. Blood pressure, body temperature, pulse, and electrocardiogram were monitored before the administration of  $^{18}\text{F}$ -RGD-K5, after the first and second PET/CT scans, and at 24 h after dose administration.

Blood and urine were collected before the drug injection and in the breaks between the PET scans. Urine was also collected at the

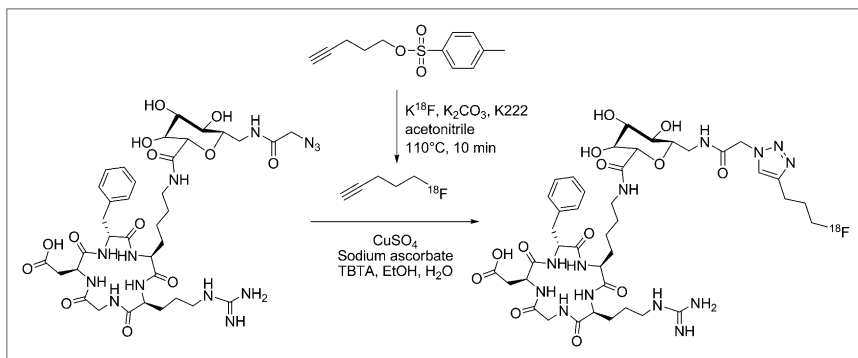


**FIGURE 2.** Synthesis of  $^{18}\text{F}$ -RGD-K5 from precursor.

end of the last PET scan. Samples of urine were assayed in a well counter to estimate the excreted activity in urine. HPLC was performed to determine the amounts of intact  $^{18}\text{F}$ -RGD-K5 and its radioactive metabolites in the plasma. Briefly, the radioactivity of the whole-blood samples was measured in a well counter in counts per minute. The whole blood was centrifuged at 3,500 rpm for 5 min to separate plasma from whole cells. The plasma fraction was removed and placed in a separate, empty, preweighed tube to record the weight of plasma. An aliquot of plasma (400  $\mu\text{L}$ ) was removed, followed by spiking of the aliquot with nonradioactive RGD-K5 standard (80  $\mu\text{L}$  of 2.5 mg/mL) and acetonitrile (400  $\mu\text{L}$ ). After the sample was stirred in a vortex mixer for 30 s and centrifuged at 13,000 rpm for 8 min to separate proteins from plasma, the plasma supernatant was removed and weighed and the counts per minute of pellet and extract were measured. An aliquot (50–100  $\mu\text{L}$ ) of the processed plasma sample was injected onto the radio-HPLC column. The radio-HPLC conditions were B = 0.1% trifluoroacetic acid in water; D = 0.1% trifluoroacetic acid in MeCN; t = 0 min 95% B, 5% D; t = 19 min 70%B, 30%D; t = 21 min 5%B, 95% D; flow, 2 mL/min; and wavelength, 206 nm. The radio-HPLC eluent was collected in 1-min fractions and individually counted. No attempts were made to identify the radioactive metabolites in the plasma or urine.

The PET scans were reconstructed to a 50-cm display field of view using an ordered-subsets expectation maximization algorithm with 28 subsets and 2 iterations. The reconstruction included corrections for random coincidences and scatter. Attenuation correction was applied on the basis of the low-dose CT. The accuracy of the activity in the PET images was verified by summing the activity in the first WB PET scan and the PET scan from mid thigh to toes and comparing it with the decayed injected activity.

The PET images for the middle time point for each patient were displayed on an imaging workstation. For each organ—including the brain, kidneys, bladder, liver, gallbladder, and large intestine (upper and lower)—volume regions of interest (ROIs) were drawn. For the small intestine, which was not visualized above background, a volume ROI was determined by marking the boundaries of visualized adjacent organs. The PET images for other time points were displayed and registered with this PET scan to transfer the volume ROI and determine the total activity in the organs. Adjustments to the individual ROIs were made to ensure the inclusion of visualized organs (e.g., bladder, gallbladder). The percentage injected activity was determined for the organs for each of the time points. The decay-corrected percentage administered activity for the top 3 organs are shown in Figure 3.

**[Fig. 3]** activity for the top 3 organs are shown in Figure 3.

### Normalized Number of Disintegrations

The percentage administered activity for each organ for each time point was fitted to an exponential or sum-of-exponentials function in OLINDA/EXM software (8) to determine the total number of disintegrations per unit administered activity, hereafter referred to as normalized number of disintegrations. Activity in the remainder of the body was calculated for each time point as the injected activity minus the activity in all the source organs and in collected urine. The half-times for biologic excretion were computed by exponential fitting of injected activity minus accumulated urine activity as a function of time. The 1- and 4.8-h bladder-voiding models in OLINDA/EXM were used to determine the normalized number of disintegrations in the bladder. Absorbed doses in the various organs were calculated by entering the normalized number of disintegrations of all source organs for each subject into OLINDA/EXM, using the standardized adult male and female models.

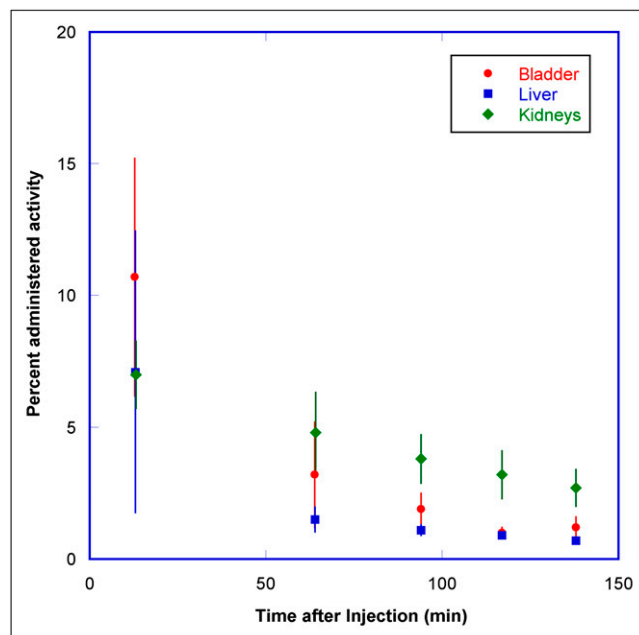


**FIGURE 3.** Mean percentage administered activity and SD for top 3 organs determined on basis of four  $^{18}\text{F}$ -RGD-K5 PET emission scans in human volunteers, as function of time after injection. Rapid clearance of activity was observed in organs.

RGB

## Animal Subjects

The rhesus monkey studies were approved by the West Point Institutional Animal Care and Use Committee at Merck Research Laboratories. Three male rhesus monkeys (ages, 7, 9, and 11 y) were initially anesthetized with ketamine (10 mg/kg intramuscularly), then induced with propofol (5 mg/kg intravenously), intubated, and ventilated with medical-grade air. Anesthesia was maintained with propofol (0.4 mg/kg/min) for the duration of the study, and the vital signs (electrocardiogram, expired tidal CO<sub>2</sub>, SPO<sub>2</sub>, and temperature) were monitored and maintained in the reference range for the duration of the study. Animals were administered an intravenous bolus of 167 ± 19 MBq of <sup>18</sup>F-RGD-K5 in a 3 mL-volume injected with a 10- to 15-s bolus duration.

## PET/CT Acquisition

After the injection of 167 ± 19 MBq of <sup>18</sup>F-RGD-K5 to the monkeys, low-dose unenhanced CT (120 kVp, 60 mA, 0.5-s rotation, and 3.75-mm slice thickness) was performed, followed by dynamic whole-body PET on a Discovery ST (GE Healthcare) PET/CT scanner. Twenty-four WB PET images were acquired in 2-dimensional mode for 5 bed positions covering 72.9 cm axially for a total duration of 200 min (time per bed range, 15 s to 4 min).

After the completion of WB PET, contrast-enhanced CT (200 mA, 120 kVp, 0.5-s rotation, and 3.75-mm slice thickness) using iohexol (Omnipaque 300; GE Healthcare) (2.5 mL/kg) was performed to assist with organ identification.

## Data Analysis

The PET scans were reconstructed using an ordered-subsets expectation maximization algorithm with 30 subsets and 2 iterations and a gaussian postprocessing filter of 3 mm in full width at half maximum. The reconstruction included corrections for scatter and random coincidences. Attenuation correction was applied on the basis of the low-dose CT.

For each study, ROIs were delineated using both the enhanced CT and the summed PET. ROIs included the brain (CT), heart content (first PET), liver (summed PET), spleen (CT), kidneys (CT), testes (CT), and urinary bladder (last PET). The gut ROI was drawn around the abdomen, excluding all other delineated organs. As such, the gut ROI included the gallbladder. ROIs were projected onto the PET images at each time point. Time-activity curves were obtained by calculating the total activity in the ROIs and expressing them as percentage of the total injected activity.

## Absorbed Dose Calculations

The percentage administered activity in each source organ was iteratively fitted to a biexponential function using a nonlinear least-squares regression algorithm (SAAM II, version 1.2, software) (9) to obtain the normalized number of disintegrations for important source organs.

Rhesus monkeys accumulated radioactivity in the urinary bladder over the duration of the study. The percentage administered activity in the bladder, obtained from the monkey images, was used as input, and the number of disintegrations from the urinary bladder's contents was calculated using the dynamic bladder model of Cloutier et al. (10). Bladder-voiding intervals of 1 and 4.8 h were used.

In this analysis, the gut ROI comprised the gallbladder, small bowel, upper large intestine, and lower large intestine. The value for fecal excretion fraction ( $f_{\text{gut}}$ ) was taken as the value at the last image time (≈200 min). The gut residence times were calculated using the model for gastrointestinal tract kinetics from the Inter-

national Commission on Radiation Protection publication 30 (11), assuming the radioactivity entered via the small bowel.

To obtain an estimate of the corrected total-body time-activity curve (which excluded the activity in the gut and bladder), the total-body time-activity curve was first constructed as decay-corrected injected activity minus the urinary excreted activity and was fit to a biexponential function. Second, to correct the total-body time-activity curve for fecal excretion, the total-body curve was also multiplied by a factor of  $1 - f_{\text{gut}}$ , where  $f_{\text{gut}}$  is the fecal excretion fraction. The corrected total-body number of disintegrations was calculated by integrating the corrected total-body time-activity curve fit. The remainder of the body number of disintegrations was calculated as the corrected total-body number of disintegrations minus all other disintegrations, except the bladder and gut.

Human radiation doses were calculated from these rhesus monkey normalized number of disintegrations using OLINDA/EXM for the adult male and female phantoms. No scaling of the rhesus biodistribution data was done to estimate human absorbed radiation doses. Thus, it was assumed that the biodistribution in these monkeys was the same as in humans.

## RESULTS

### Human Studies

The injection of 583 ± 78 MBq of <sup>18</sup>F-RGD-K5 in 3 subjects produced no clinically significant effects on vital signs (blood pressure, temperature, pulse, and electrocardiogram) and blood tests during the 2.5-h observation period after administration and in the follow-up visit at 24 h.

The analysis of plasma samples of 2 subjects showed that the level of unmetabolized <sup>18</sup>F-RGD-K5 in the plasma remained constant (>95% intact) over 90 min after injection, consistent with human metabolism data reported for this class of compounds (5). <sup>18</sup>F-RGD-K5 exhibited a plasma clearance half-time of approximately 12 min.

Figure 4 displays PET maximum-intensity-projection [Fig. 4] images for 1 of the subjects from the PET scans. In the first scan, the predominant uptake was seen in the urinary bladder, with moderate uptake in the liver and kidneys. The gallbladder and small intestine displayed <sup>18</sup>F-RGD-K5 uptake in later scans. All other organs had a near-background level of activity. Mean standardized uptake values at about 1 h after injection were approximately 50 in bladder, 20 in kidneys, 10 in gallbladder, and 4 in liver. The rest of the body had low standardized uptake values. The percentage administered activity for the top 3 organs is shown in Fig. [Fig. 5] 5. There was large intersubject variation in the bladder uptake (6.4%–12.4%) and kidney uptake (3%–14%), as indicated by the large error bars. The renal system (kidneys and bladder together) had more consistent uptake, ranging from 18.4% to 20.4%. The liver had the next highest uptake, ranging from 6.2% to 8.7%. The study drug was excreted primarily via the renal system. By the end of the study (~2.5 h), approximately 44% of the injected activity of <sup>18</sup>F-RGD-K5 had been excreted in the urine, as determined by assaying urine samples in a well counter.

The normalized number of disintegrations for the organs is listed in Table 1. The mean organ doses are given in [Table 1]

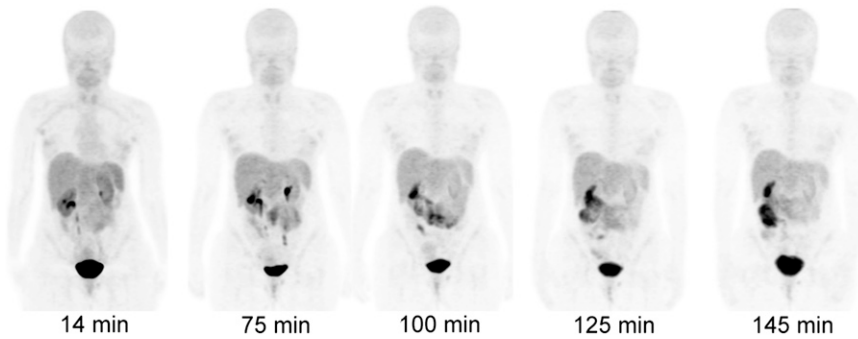


**FIGURE 4.** Decay-corrected anterior maximum-intensity projections of PET at 14, 75, 100, 125, and 145 min after injection of  $^{18}\text{F}$ -RGD-K5 in female volunteer. There was rapid clearance of activity in kidneys, liver, and bladder. Gallbladder activity peaked at 75 min and then decreased with time.

**[Table 2]** Table 2. The mean effective dose of  $^{18}\text{F}$ -RGD-K5 for the human adult male phantom was  $15 \pm 1$  and  $31 \pm 1$   $\mu\text{Sv}/\text{MBq}$  for the 1- and 4.8-h bladder-voiding models, respectively. For a typical 555-MBq injected dose of  $^{18}\text{F}$ -RGD-K5, the WB effective dose for the 2 models would be  $8.3 \pm 0.6$  and  $17.2 \pm 0.6$  mSv, respectively. The adult female phantom doses were typically approximately 25% higher. The 3 organs with the highest radiation absorbed doses were urinary bladder wall, gallbladder wall, and kidneys.

### Monkey Studies

The injection of  $167 \pm 19$  MBq of  $^{18}\text{F}$ -RGD-K5 in 3 male monkeys produced no clinically significant effects on vital signs (blood pressure, pulse, and electrocardiogram) and blood tests during the 3-h observation period after administration. In the rhesus monkey, the liver was best visualized at approximately 37 min after injection, whereas the bladder content became visible at approximately 10 min after injection.

The PET maximum-intensity-projection images at 1, 13, 42.6, 111.5, and 190 min after injection are shown in Figure 6. At 3 min, rapid uptake of  $^{18}\text{F}$ -RGD-K5 was observed in the heart, kidneys, and liver. The bladder's activity accumulated over time, because the rhesus monkeys were under anesthesia and did not void. Gallbladder uptake was observed at later time points. Rapid clearance of activity in the kidneys and liver was observed in the images at subsequent time points. The urinary bladder had the highest uptake, with  $55\% \pm 12\%$  of injected activity at the end of the 3-h PET/CT acquisition. The peak values of percentage administered activity in the liver, kidneys, and brain were  $7.6\% \pm 1.2\%$ ,  $6.6\% \pm 2.7\%$ , and  $0.42\% \pm 0.1\%$ , respectively, at 3–4 min after injection. At the end of the study,  $9.1\% \pm 1.6\%$  of injected activity was found in the gut, which included the gallbladder, small intestine, and upper and lower portions of the large intestine.

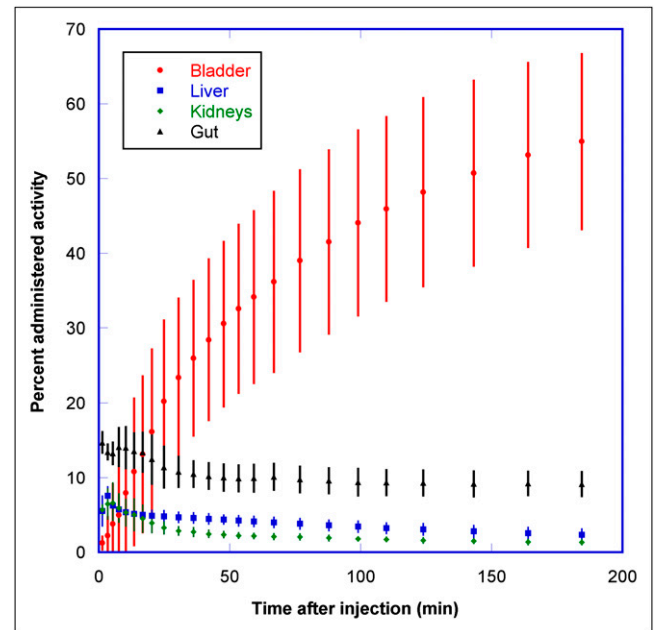
The normalized number of disintegrations for the organs is listed in Table 3. The mean organ doses for the male human phantom estimated using primate  $^{18}\text{F}$ -RGD-K5 biodistribution are given in Table 4. The 4 organs with the highest radiation-absorbed doses were the urinary bladder wall, upper large intestine wall, small intestine, and testes. The mean effective dose of  $^{18}\text{F}$ -RGD-K5 was  $23 \pm 0.3$  for the 1-h and  $40 \pm 4.4$   $\mu\text{Sv}/\text{MBq}$  for the 4.8-h bladder-void-

ing models. The estimated doses for the female human phantom were higher by approximately 25%.

### DISCUSSION

$^{18}\text{F}$ -RGD-K5, developed as an integrin marker, was investigated in this dosimetry study in both humans and monkeys. The findings from this investigation show substantial promise of  $^{18}\text{F}$ -RGD-K5 as a PET agent, with a reasonable biodistribution and safety profile in human subjects. This study provides information on the background uptake levels in normal organs. The data also assess the potential radiation exposure in humans through WB PET in humans and monkeys.

In humans,  $^{18}\text{F}$ -RGD-K5 revealed a biodistribution dominated by activity in the bladder, kidneys, and liver and steady renal clearance, with 44% of injected activity excreted within the 2.5-h duration of the study. In the inter-



RGB

**FIGURE 5.** Mean percentage administered activity and SD for top 4 organs determined on basis of 3 rhesus monkey  $^{18}\text{F}$ -RGD-K5 PET emission scans, as function of time after injection. Liver and kidney activities decreased rapidly with time, and bladder activity increased with time (there was no voiding because monkeys were anesthetized).

**TABLE 1**

Normalized Number of Disintegrations of Source Organs for Human Subjects Injected with  $^{18}\text{F}$ -RGD-K5

Organ	Normalized no. of disintegrations (MBq-h/MBq administered)
Brain	0.021 ± 0.003
Gallbladder contents	0.058 ± 0.038
Kidneys	0.065 ± 0.016
Liver	0.171 ± 0.043
Lower large intestine	0.015 ± 0.009
Small intestine	0.036 ± 0.016
Upper large intestine wall	0.031 ± 0.047
Urinary bladder contents (1 h)	0.205 ± 0.01
Urinary bladder contents (4.8 h)	0.781 ± 0.041
Remainder	1.15 ± 0.096

Data are mean ± SD;  $n = 4$ .

mediate and late scans, gallbladder and small intestine activity was observed. The relatively wide range of activities seen in the various organs implies a wide range of absorbed radiation doses. The urinary bladder, liver, kidneys, gallbladder, and small intestine had radioactivity levels greater than background radioactivity.

Among all the organs observed, the urinary bladder received the highest dose in the 4.8-h bladder-voiding model. The mean urinary bladder wall dose was  $103 \pm 4$  and  $376 \pm 19$   $\mu\text{Gy}/\text{MBq}$  for the 1- and 4.8-h bladder-voiding models, respectively. The gallbladder and kidneys had the next highest doses:  $104 \pm 52$  for the 1-h model and  $45 \pm 10$   $\mu\text{Gy}/\text{MBq}$  for the 4.8-h model. The remaining organs had lower doses, in the range of 5–32  $\mu\text{Gy}/\text{MBq}$ . The average values of effective dose for  $^{18}\text{F}$ -RGD-K5 were  $15 \pm 1$  and  $31 \pm 1$   $\mu\text{Sv}/\text{MBq}$ , respectively, for the 2 models. For a typical 555-MBq injected dose of  $^{18}\text{F}$ -RGD-K5, the effective dose for the 4.8-h model is  $17.2 \pm 0.6$  mSv. The effective dose was lower than the 30-mSv WB dose limit specified by the Food and Drug Administration for research subjects (12). The doses can be reduced by more frequent

**TABLE 2**

Radiation Dosimetry Estimates per Unit Administered Activity for  $^{18}\text{F}$ -RGD-K5 for Human Adult Male Phantom in 1- and 4.8-Hour Bladder-Voiding Models, Based on Human Biodistribution Data

Organ	1-h void model ( $\mu\text{Gy}/\text{MBq}$ )	4.8-h void model ( $\mu\text{Gy}/\text{MBq}$ )
Urinary bladder wall	103 ± 4	376 ± 19
Gallbladder wall	103 ± 58	104 ± 59
Kidneys	45 ± 10	45 ± 10
Uterus	14 ± 0.3	31 ± 1
Lower large intestine wall	19 ± 5	27 ± 5
Liver	25 ± 5	26 ± 5
Upper large intestine wall	22 ± 18	25 ± 17
Small intestine	17 ± 2	20 ± 2
Ovaries	11 ± 1	19 ± 0.5
Testes	7.5 ± 0.4	13 ± 0.1
Pancreas	10 ± 1	10 ± 1
Osteogenic cells	10 ± 1	10 ± 1
Adrenals	10 ± 1	10 ± 1
Muscle	7 ± 0.4	9 ± 0.3
Stomach wall	8.2 ± 1	8.6 ± 0.5
Red marrow	6.9 ± 0.4	8.2 ± 0.3
Spleen	7.9 ± 0.3	8.2 ± 0.3
Heart wall	7.4 ± 0.4	7.5 ± 0.4
Lungs	6.6 ± 0.4	6.6 ± 0.4
Thymus	6.1 ± 0.4	6.2 ± 0.4
Thyroid	5.9 ± 0.5	5.9 ± 0.5
Skin	5 ± 0.3	5.7 ± 0.3
Breasts	5.1 ± 0.3	5.2 ± 0.3
Total body	7.8 ± 0.4	9.6 ± 0.3
Effective dose ( $\mu\text{Sv}/\text{MBq}$ )	15 ± 1	31 ± 1

Data are mean ± SD;  $n = 4$ .

bladder voiding. For the 1-h bladder-voiding model, the WB effective dose reduces to  $8.3 \pm 0.6$  mSv.

$^{18}\text{F}$ -RGD-K5 was found to be intact in human plasma up to 90 min after injection. This result is consistent with the metabolic profile of other RGD-containing PET tracers in human plasma (5). One possible explanation for the stability of this tracer in vivo is the rapid clearance of the tracer through the renal system, with relatively little exposure time within the liver.

**FIGURE 6.** Decay-corrected anterior maximum-intensity projections of PET at 1, 13, 42.6, 111.5, and 190 min after injection of  $^{18}\text{F}$ -RGD-K5 in rhesus monkey. Liver and kidney activities decreased rapidly with time, and bladder and rectum accumulated activity with time (there was no voiding of bladder because monkey was anesthetized).

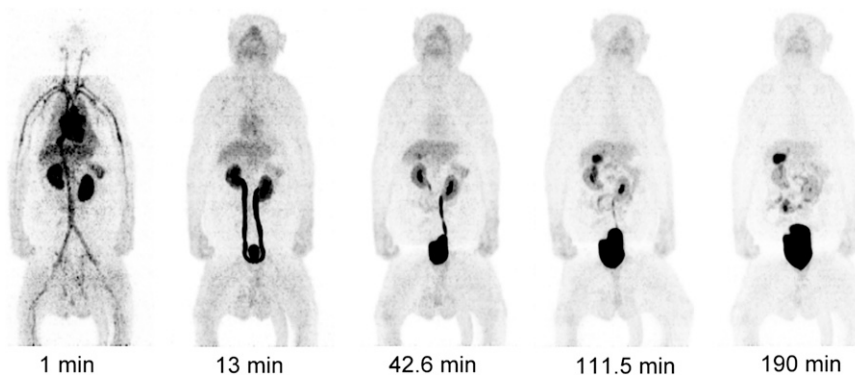


TABLE 3

Normalized Number of Disintegrations of Source Organs for Rhesus Monkeys Injected with  $^{18}\text{F}$ -RGD-K5

Organ	Normalized no. of disintegrations (MBq-h/MBq administered)
Brain	0.0054 ± 0.0018
Heart contents	0.025 ± 0.0073
Kidneys	0.054 ± 0.0092
Liver	0.085 ± 0.0153
Lower large intestine	0.028 ± 0.0033
Small Intestine	0.28 ± 0.033
Upper large intestine wall	0.15 ± 0.018
Spleen	0.0062 ± 0.0035
Testes	0.0092 ± 0.0004
Urinary bladder contents (1 h)	0.22 ± 0.06
Urinary bladder contents (4.8 h)	0.83 ± 0.21
Remainder	1.39 ± 0.23

Data are mean ± SD;  $n = 3$ .

In monkeys,  $^{18}\text{F}$ -RGD-K5 showed a biodistribution dominated by activity in the kidney and bladder and steady renal clearance, with  $17\% \pm 2\%$  of injected activity excreted in the 3 h of the study. In the intermediate scans, rapid clearance of activity was observed in all the organs, and intestinal elimination as indicated by gut activity was also observed. The liver, kidneys, and heart contained above-background activities in the early stages after injection, with the gallbladder and gut activity accumulating at later time points. Mean standardized uptake values 1 h after injection were approximately 2 in liver and approximately 6 in the kidneys and gallbladder.

For the human adult male model, only the urinary bladder wall was estimated to receive radiation doses larger than  $100 \mu\text{Gy}/\text{MBq}$ . The mean bladder wall dose was 110 and  $400 \mu\text{Gy}/\text{MBq}$  for 1- and 4.8-h bladder-voiding intervals, respectively. Upper large intestine wall and small intestines received the next highest doses. The mean values of the effective dose for the human adult male model were  $23 \pm 0.3 \mu\text{Sv}/\text{MBq}$  (1-h voiding interval) and  $40 \pm 4.4 \mu\text{Sv}/\text{MBq}$  (4.8-h voiding interval).

The monkey data included fast-sampling or dynamic PET scans (15 s per bed position) during the first few minutes, followed by longer PET scans (4 min per bed position). The human data did not include the fast sampling but consisted of sequential WB PET scans at 6 min per bed position. A comparison of dosimetry for another  $^{18}\text{F}$ -based imaging agent using similar datasets has shown that consistent dosimetry results were obtained without the fast sampling (13). Hence, the comparison of results between monkey and human data may be justified despite differences in the acquisition parameters.

There were many similarities between the monkey and human biodistribution and dosimetry data. In both human and monkey datasets, the organs with the highest normal-

TABLE 4

Radiation Dosimetry Estimates per Unit Administered Activity for  $^{18}\text{F}$ -RGD-K5 for Human Adult Male Phantom in 1- and 4.8-Hour Bladder-Voiding Models, Based on Primate Biodistribution Data

Organ	1-h void model ( $\mu\text{Gy}/\text{MBq}$ )	4.8-h void model ( $\mu\text{Gy}/\text{MBq}$ )
Urinary bladder wall	110 ± 65	400 ± 100
Upper large intestine wall	74 ± 8.3	77 ± 8.5
Small intestine	66 ± 6.8	69 ± 6.9
Testes	44 ± 2.3	49 ± 2.0
Kidneys	38 ± 6.2	39 ± 6.2
Uterus	19 ± 0.3	37 ± 4.6
Lower large intestine wall	29 ± 2.0	38 ± 2.3
Ovaries	18 ± 1.2	26 ± 1.2
Liver	14 ± 2.5	15 ± 2.4
Gallbladder wall	13 ± 1.8	14 ± 1.7
Spleen	11 ± 4.2	11 ± 4.0
Heart wall	11 ± 2.6	11 ± 2.5
Osteogenic cells	8.2 ± 1.7	9.0 ± 1.4
Stomach wall	8.6 ± 1.4	9.0 ± 1.4
Pancreas	8.6 ± 1.6	8.9 ± 1.6
Muscle	6.7 ± 1.0	8.8 ± 0.4
Red marrow	7.1 ± 1.0	8.5 ± 0.7
Adrenals	7.9 ± 1.5	8.1 ± 1.5
Lungs	5.3 ± 1.2	5.3 ± 1.2
Thymus	5.3 ± 1.2	5.3 ± 1.2
Skin	4.3 ± 0.8	5.1 ± 0.7
Thyroid	4.6 ± 1.1	4.6 ± 1.2
Breast	4.2 ± 1.0	4.2 ± 1.0
Brain	1.9 ± 0.6	1.9 ± 0.6
Total body	7.8 ± 1.1	9.7 ± 0.6
Effective dose ( $\mu\text{Sv}/\text{MBq}$ )	23 ± 0.3	40 ± 4.4

Data are mean ± SD;  $n = 3$ .

ized number of disintegrations of  $^{18}\text{F}$ -RGD-K5 were the urinary bladder, liver, and kidneys. In addition, in both cases the bladder wall received the highest dose. In both datasets, the various organs of the digestive tract had similar dose levels. For humans, the doses ranged from 6 to  $64 \mu\text{Gy}/\text{MBq}$ , whereas for monkeys, the doses ranged from 9 to  $75 \mu\text{Gy}/\text{MBq}$ . The effective dose was  $40 \pm 4.4 \mu\text{Sv}/\text{MBq}$  for monkey-derived estimates and  $31 \pm 1 \mu\text{Sv}/\text{MBq}$  for human-based estimates in the 4.8-h bladder-voiding model. For the 1-h bladder-voiding model, the effective doses were  $23 \pm 0.3 \mu\text{Sv}/\text{MBq}$  for monkey-derived estimates and  $15 \pm 1 \mu\text{Sv}/\text{MBq}$  for human-based estimates.

Table 5 compares the doses to individual organs for  $^{18}\text{F}$ -RGD-K5,  $^{18}\text{F}$ -FDG (14),  $^{18}\text{F}$ -HX4 (15), and  $^{18}\text{F}$ -fluoromisonidazole (4-h bladder-voiding model) (16,17). The absorbed doses in the heart, brain, and breasts were much lower for  $^{18}\text{F}$ -RGD-K5 than for  $^{18}\text{F}$ -FDG.  $^{18}\text{F}$ -RGD-K5 did not appreciably cross the blood-brain barrier in our imaging studies. The absorbed doses in urinary bladder, liver, and kidneys were higher for  $^{18}\text{F}$ -RGD-K5 than for  $^{18}\text{F}$ -FDG. A large fraction of  $^{18}\text{F}$ -RGD-K5 ( $\sim 44\%$  in 2.5 h) and  $^{18}\text{F}$ -HX4 ( $\sim 45\%$  in 3.5 h) was excreted through the urinary system,

**TABLE 5**  
Organ Doses in  $\mu\text{Gy}/\text{MBq}$  for Several  $^{18}\text{F}$ -Based Imaging Agents

Organ	RGD-K5	$^{18}\text{F}$ -FDG	Galacto-RGD	Fluoromisonidazole	HX4
Adrenals	10	13	5.4	16.6	9.6
Brain	4.8	19	1.5	8.6	5
Breasts	5.2	9.2	2	12.3	6
Gallbladder wall	104	14	7.6	14.8	24
Heart wall	7.5	60	3.5	18.5	9
Kidneys	45	20	29.5	15.7	20
Liver	26	16	23	18.3	14
Lower large intestine wall	27	17	12	14.3	28
Lungs	6.6	17	6.6	9.9	8
Muscle	9	11	5.3	14.2	10
Osteogenic cells	10.3	12	3.8	7.7	12
Ovaries	19	17	11.1	17.6	18
Pancreas	10	26	5.4	17.9	10
Red marrow	8.2	13	3.9	10.9	9
Skin	5.7	8.4	2.3	4.8	7
Small intestine	20	14	15.4	13.2	17
spleen	8.2	37	16.3	16.3	9
Stomach wall	8.6	13	4.1	12.6	9
Testes	13	13	4.4	14.6	13
Thymus	6.2	12	2.5	15.5	8
Thyroid	5.9	10	2.09	15.1	8
Upper large intestine wall	25	13	16	14	18
Urinary bladder wall	376	190	218	29	299
Uterus	31	23	17.4	18.3	28

RG-K5,  $^{18}\text{F}$ -FDG, and HX4 data use 4.8-h bladder-voiding model; galacto-RGD uses 2-h bladder-voiding model; and fluoromisonidazole data use 4-h bladder-voiding model.

whereas  $^{18}\text{F}$ -fluoromisonidazole had little urinary excretion ( $\sim 4\%$  in 5 h). Hence, the urinary bladder doses for  $^{18}\text{F}$ -RGD-K5 (376  $\mu\text{Gy}/\text{MBq}$ ) and  $^{18}\text{F}$ -HX4 (299  $\mu\text{Gy}/\text{MBq}$ ) were much higher than that for  $^{18}\text{F}$ -fluoromisonidazole (29  $\mu\text{Gy}/\text{MBq}$ ) (for 4-h bladder-voiding model). However, steps can be taken to reduce the bladder dose. Patients can be encouraged to void frequently because the bladder dose reduced to approximately  $103 \pm 4 \mu\text{Gy}/\text{MBq}$  in the 1-h bladder-voiding model.

**[Table 6]** Table 6 compares WB radiation dose and effective dose from  $^{18}\text{F}$ -RGD-K5 with doses from a few  $^{18}\text{F}$ -based radiopharmaceuticals (14,16,17). As shown in these tables, the radiation dose from  $^{18}\text{F}$ -RGD-K5 is comparable to that from other  $^{18}\text{F}$ -based imaging agents.

## CONCLUSION

The biodistribution profile of  $^{18}\text{F}$ -RGD-K5 was similar for monkeys and humans. For a typical 555-MBq injected dose of  $^{18}\text{F}$ -RGD-K5, the effective dose for the 4.8- and 1-h bladder-voiding models was  $17.2 \pm 0.6$  and  $8.3 \pm 0.6$  mSv, respectively. The urinary bladder wall had the highest dose among all the organs and is deemed to be the critical organ. With frequent bladder voiding, doses to the bladder and the WB can be reduced.  $^{18}\text{F}$ -RGD-K5 can be used safely in humans for imaging integrin  $\alpha_v\beta_3$  expression.

## DISCLOSURE STATEMENT

The costs of publication of this article were defrayed in part by the payment of page charges. Therefore, and solely

**TABLE 6**  
Comparison of Dose per Unit Administered Activity Between  $^{18}\text{F}$ -RGD-K5 and Other  $^{18}\text{F}$ -Based Imaging Agents

Dose	RGD-K5, 1-h bladder-voiding interval	RGD-K5, 4.8-h bladder-voiding interval	$^{18}\text{F}$ -FDG, 4.8-h bladder-voiding interval	Galacto-RGD, 2-h bladder-voiding interval	HX4, 1-h bladder-voiding interval	HX4, 4.8-h bladder-voiding interval
Total body dose ( $\mu\text{Gy}/\text{MBq}$ )	7.8	9.6	11	5.34	8	10
Effective dose ( $\mu\text{Sv}/\text{MBq}$ )	15	31	19	18.68	14	27



to indicate this fact, this article is hereby marked “advertisement” in accordance with 18 USC section 1734.

## ACKNOWLEDGMENTS

We thank Donna Mosley for her help with patient data acquisition. We thank Mary Benetz and the staff from the Protocol Management Office, Clinical Research Unit, and Protocol Support Laboratory for their help with the research protocol. In addition, we thank Stephen M. Krause, Merck and Co., for the rhesus monkey data acquisition. The study was supported by Siemens Molecular Imaging Inc. The human part of the study was conducted at Fox Chase Cancer Center under the ClinicalTrials.gov Identifier NCT00743353. No other potential conflict of interest relevant to this article was reported.

## REFERENCES

1. Brown AP, Citrin DE, Camphausen KA. Clinical biomarkers of angiogenesis inhibition. *Cancer Metastasis Rev*. 2008;27:415–434.
2. Brooks PC, Montgomery AM, Rosenfeld M, et al. Integrin alpha v beta 3 antagonists promote tumor regression by inducing apoptosis of angiogenic blood vessels. *Cell*. 1994;79:1157–1164.
3. Gasparini G, Brooks PC, Biganzoli E, et al. Vascular integrin  $\alpha_v\beta_3$ : a new prognostic indicator in breast cancer. *Clin Cancer Res*. 1998;4:2625–2634.
4. Vonlaufen A, Wiedle G, Borisch B, Birrer S, Luder P, Imhof BA. Integrin  $\alpha_v\beta_3$  expression in colon carcinoma correlates with survival. *Mod Pathol*. 2001;14:1126–1132.
5. Beer AJ, Haubner R, Wolf I, et al. PET-based human dosimetry of  $^{18}\text{F}$ -galacto-RGD, a new radiotracer for imaging  $\alpha_v\beta_3$  expression. *J Nucl Med*. 2006;47:763–769.
6. Haubner R, Kuhnast B, Mang C, et al. [ $^{18}\text{F}$ ]Galacto-RGD: synthesis, radiolabeling, metabolic stability, and radiation dose estimates. *Bioconjug Chem*. 2004;15:61–69.
7. Walsh JC, Kolb HC. Applications of click chemistry in radiopharmaceutical development. *Chimia (Aarau)*. 2010;64:29–33.
8. Stabin MG, Sparks RB, Crowe E. OLINDA/EXM: the second-generation personal computer software for internal dose assessment in nuclear medicine. *J Nucl Med*. 2005;46:1023–1027.
9. Barrett PH, Bell BM, Cobelli C, et al. SAAM II: Simulation, analysis, and modeling software for tracer and pharmacokinetic studies. *Metabolism*. 1998;47:484–492.
10. Cloutier RJ, Smith SA, Watson EE, Snyder WS, Warner GG. Dose to the fetus from radionuclides in the bladder. *Health Phys*. 1973;25:147–161.
11. International Commission on Radiological Protection (ICRP). Limits of intake of radio-nuclides by workers. Publication 30. *Ann ICRP*. 1979;2.
12. Food and Drug Administration (FDA). Guidance for Industry and Researchers, The Radioactive Drug Research Committee: Human Research Without an Investigational New Drug Application. August 2010. Available at: <http://www.fda.gov/downloads/Drugs/GuidanceComplianceRegulatoryInformation/Guidances/UCM163892.pdf>. Accessed April 2, 2012.
13. Herzog H, Elmenhorst D, Winz O, Bauer A. Biodistribution and radiation dosimetry of the A1 adenosine receptor ligand  $^{18}\text{F}$ -CPFPX determined from human whole-body PET. *Eur J Nucl Med Mol Imaging*. 2008;35:1499–1506.
14. Stabin M, Stubbs J, Toohey R. Radiation dose estimates for radiopharmaceuticals, NUREG/CR-6345. April 1996. Available at: <http://www.nrc.gov/reading-rm/doc-collections/nuregs/contract/cr6345/cr6345.pdf>. Accessed April 2, 2012.
15. Doss M, Zhang JJ, Belanger MJ, et al. Biodistribution and radiation dosimetry of the hypoxia marker  $^{18}\text{F}$ -HX4 in monkeys and humans determined by using whole-body PET/CT. *Nucl Med Commun*. 2010;31:1016–1024.
16. Graham MM, Peterson LM, Link JM, et al. Fluorine-18-fluoromisonidazole radiation dosimetry in imaging studies. *J Nucl Med*. 1997;38:1631–1636.
17. Tolvanen T, Lehtio K, Kulmala J, et al.  $^{18}\text{F}$ -Fluoroerythronitroimidazole radiation dosimetry in cancer studies. *J Nucl Med*. 2002;43:1674–1680.